INTERNATIONAL JOURNAL FOR NUMERICAL METHODS IN FLUIDS, VOL. 7, 1235–1259 (1987)

ON A FINITE ELEMENT CFD ALGORITHM FOR COMPRESSIBLE, VISCOUS AND TURBULENT AERODYNAMIC FLOWS*

A. J. BAKER, J. W. KIM

Department of Engineering Science and Mechanics, University of Tennessee, Knoxville, TN 37996-2030, U.S.A.

J. D. FREELS

Technology for Energy Corporation, Knoxville, TN, U.S.A.

AND

J. A. ORZECHOWSKI

Computational Mechanics Corporation, Knoxville, TN, U.S.A.

SUMMARY

This paper develops and analyses individual construction aspects of an efficient and accurate finite element algorithm for prediction of viscous and turbulent flow fields of impact in aerodynamics. The theoretical construction employs a Taylor weak statement (TWS) for coincident embedding of stability mechanisms within a classic Galerkin finite element formulation of semi-discrete approximation error orthogonalization. A wide variety of the stabilizing mechanisms of independently derived CFD algorithms are contained within the TWS theory. An implicit construction that meets the requirement of efficient convergence to steady state is developed. The theoretical asymptotic error estimates of the TWS finite element algorithm for supersonic and viscous boundary layer flows are verified. Application to a three-dimensional turbulent flow is cited.

KEY WORDS Fluid Mechanics CFD Finite Element Accuracy/Convergence Stability PNS/TLNS Turbulent

INTRODUCTION

The unsteady three-dimensional Navier–Stokes (3 DNS) equations for a viscous, compressible, heat-conducting fluid are the pertinent system governing aerodynamics. The direct solution of the 3 DNS system is impractical, since the number of floating point operations for a grid of sufficient refinement (to predict details accurately) exceeds even next-generation supercomputer capabilities. Therefore, simplifications to the 3 DNS system for numerical approximation have been the subject of CFD algorithm research over the past two decades. For steady, three-dimensional aerodynamic flows, a modestly restricted but highly useful simplification is the 'thin layer Navier–Stokes (TLNS)' approximation, wherein axial diffusion effects (in the direction parallel to the predominant flow direction) are neglected as higher order. This singular perturbation approximation does not in itself impose a pressure approximation, and the pressure field exerts an (elliptic) boundary-value character for all but purely supersonic inviscid flows. Hence, only in this special case is the steady

* Based as an invited lecture.

0271–2091/87/111235–25$12.50

flow TLNS set mathematically well posed as a (spatial) initial-value problem.

The accounting of the elliptic pressure coupling for a viscous/turbulent flow prediction is the *principal distinguishing characteristic* of the many published finite difference (FD), approximate factorization (AF), finite volume (FV) and finite element (FE) space-marching 'parabolic Navier–Stokes (PNS)' algorithms for solution of the steady TLNS equation set. Problem well-posedness, and the inclusion of downstream pressure (signals) within subsonic/transonic regions, requires algorithm construction within a pressure interaction framework. Rubin and co-workers[1–5] pioneered early developments, and Rubin[6] reviews procedures for pressure interaction and relaxation procedures for separated incompressible flows. Lin and Rubin[7] present a strongly implicit (CSIP) PNS algorithm for supersonic viscous external flows utilizing a global relaxation for the pressure interaction that eliminates the 'departure solution', the viscous PNS algorithm lower-bound stability constraint on axial (marching) step size. Reddy and Rubin[8] document the subsonic/transonic 2D extension of the CSIP relaxation PNS algorithm for shocked aerofoil flows exhibiting strong pressure interaction.

Vigneron *et al.*[9] first reported a non-iterative AF PNS algorithm for 3D TLNS in stretched Cartesian co-ordinates for sharp cones. Rakich *et al.*[10] generalized the co-ordinate system and included a turbulent capability using an elementary eddy viscosity model. For the reported solutions, the axial pressure gradient was usually neglected and mention is made of the need to add artificial viscosity terms for stabilization. An analysis is reported that predicts the fraction ω of the axial pressure gradient that can be implicitly included in the subsonic regions for steady flow while maintaining algorithm stability. Tannehill *et al.*[11] generalize the AF non-iterative PNS algorithm to supersonic blunt body downstream flows in generalized co-ordinates and archive the departure solution stability analysis of Vigneron *et al.* The completely generalized co-ordinate transformation renders PNS solution initiation more stable, a difficulty that is reported to pervade the entire spectrum of PNS algorithm constructions.

An alternative TLNS AF algorithm is published by Schiff and Steger[12] for 2D and 3D laminar external flows in generalized co-ordinates. The delta form is detailed, as is a sublayer approximation for the axial pressure gradient and a global surface pressure iteration to suppress the departure solution. Chaussee *et al.*[13] report, for geometrically complicated blunt bodies, the extension which is conservative, first- or second-order accurate in the marching direction, second-order accurate in the transverse plane and contains an artificial viscosity formulation. The departure solution is suppressed by imposing the exterior axial pressure gradient throughout the subsonic reach of the attached boundary layer. The AFWAL PNS Code[14] for supersonic, viscous external flow fields is based upon this non-iterative AF delta form PNS algorithm. A viscous–inviscid interaction pressure relaxation procedure is not included; however, Rakich[15] developed and evaluated in 2D a pressure relaxation algorithm applicable to the AF algorithm constructions.

A linearized block-implicit (LBI) FD PNS algorithm is developed for the steady Navier–Stokes equations by Briley and McDonald.[16,17] Early applications emphasized subsonic internal flows and utilized a single-pass, axial pressure gradient computation based on an inviscid flow assumption with a viscous (drag) correction. The departure solution is thus suppressed in the absence of a viscous–inviscid interaction theory. Recent applications emphasize secondary vortex generation in curved, air-breathing engine inlet ducts.[18,19] Predictions for turbulent flows used an elementary algebraic model for the Reynolds principal shear stress, with the Launder and Spalding[20] parabolized two-equation turbulent kinetic energy-isotropic dissipation (k, ε) differential equation system. The boundary conditions for k and ε were slip–wall employing similarity (log law) boundary layer concepts to produce algebraic Dirichlet expressions at $y^+ \geqslant 30$.

No research groups in the finite element community have specifically developed supersonic flow

PNS algorithms. Baker and Orzechowski[21] (see also References 22 and 23) develop an incompressible penalty function PNS algorithm for the turbulent TLNS equation set applicable to exterior as well as interior flow geometries. The continuity equation, as a differential constraint on momentum equation solutions, is imposed directly as a penalty function. An ordering analysis prompts restructuring of the transverse momentum equations to yield a pressure Poisson equation. The associated complementary and particular solution statements facilitate a pressure interaction procedure that eliminates the departure solution. The parabolic two-equation (k, ε) turbulent closure of Launder and Spalding[20] is employed, in concert with an algebraic complete Reynolds stress equation containing length scale (van Driest) damping. This permits resolution of the laminar sublayer/transition regions of boundary and corner layers using no-slip boundary conditions.

This paper develops and examines key theoretical elements of a mixed supersonic/subsonic FE PNS algorithm for application to aerodynamic flows including turbulent and three-dimensional configurations. The principal analysis aspects include construction of a stable and efficient algorithm and the interplay between numerical and physical dissipation mechanisms and time- and/or space-marching procedures.

PROBLEM STATEMENT

Governing equation statement

The TLNS approximation is an elementary but mathematically consequential simplification of the complete 3 DNS equation system, which in non-dimensional conservation law form and in a rectangular Cartesian co-ordinate system is

$$\frac{\partial q}{\partial t}+\frac{\partial(E-E_v)}{\partial x}+\frac{\partial(F-F_v)}{\partial y}+\frac{\partial(G-G_v)}{\partial z}=0. \tag{1}$$

The dependent variable set is

$$q(\mathbf{x}, t)=(\rho, \rho u, \rho v, \rho w, \rho e)^{\mathrm{T}}.$$

E, F and G contain the non-viscous terms, e.g.

$$E(\mathbf{x}, t)=(\rho u, \rho u^2+p, \rho uv, \rho uw, (\rho e+p)u)^{\mathrm{T}},$$

while E_v, F_v, G_v contain the viscous/conduction terms, e.g.

$$E_v=(0, \sigma_{xx}, \sigma_{xy}, \sigma_{xz}, u\sigma_{xx}+v\sigma_{xy}+w\sigma_{xz}+q_x)^{\mathrm{T}}.$$

A co-ordinate transformation from $\mathbf{x}$ to η is usually invoked, whereupon the divergence operator $\partial/\partial\mathbf{x}$ is transformed to scalar components in the η boundary fitted co-ordinate system. This yields definition of the contravariant components (U_i) of the convection velocity $\mathbf{u}$, and the determinant J of the transformation Jacobian as the measure of the mesh.

The unsteady 3 DNS equation system is addressed, although we principally seek its steady state approximate solution. Equation (1) must be statistically averaged; an ensemble-averaging or mass-weighted time-averaging procedure[24] is appropriate, wherein the mean velocity definition becomes

$$\tilde{u}_i \equiv \overline{\rho u_i}/\overline{\rho}, \tag{2}$$

with the overbar denoting time average. Thereupon, we have the definitions

$$\begin{aligned}
\overline{\rho u_i} &= \bar{\rho}\tilde{u}_i, \\
\overline{\rho u_i u_j} &= \overline{\rho u_i}\,\tilde{u}_j + \overline{\rho u_i' u_j'}, \\
\overline{\rho H} &= \overline{\rho h} + \tfrac{1}{2}\overline{\rho u_i}\,\tilde{u}_i + \tfrac{1}{2}\overline{\rho u_i' u_i'}, \\
\tilde{H} &= \tilde{h} + \tfrac{1}{2}\tilde{u}_i\tilde{u}_i + \tfrac{1}{2}\overline{\rho u_i' u_i'}/\bar{\rho}, \\
\tilde{h} &= \overline{\rho h}/\bar{\rho} \equiv (\bar{p}/\rho)^{[\tilde{\gamma}/(\tilde{\gamma}-1)]},
\end{aligned} \tag{3}$$

Real gas effects may be accounted for by variable gamma,[25] wherein $\tilde{\gamma} \equiv \tilde{h}/\tilde{e}$ is the effective gamma and $\tilde{e}$ is the specific internal energy. In terms of $q \equiv (\bar{\rho}, \overline{\rho u_i}, \overline{\rho H} - \bar{p})^{\mathrm{T}}$, the 3 DNS equation system can be written as

$$\frac{\partial q}{\partial t} + \frac{\partial f_j}{\partial x_j} = 0 \tag{4}$$

and

$$f_j = \begin{pmatrix} \overline{\rho u_j} \\ \tilde{u}_j\overline{\rho u_i} + \bar{p}\delta_{ij} - (\overline{\sigma_{ij}} - \overline{\rho u_i' u_j'}) \\ \tilde{u}_j\overline{\rho H} + (\overline{q_j} + \overline{\rho H' u_j'} - \tilde{u}_i\overline{\sigma_{ij}} - \overline{u_i'\sigma_{ij}}) \end{pmatrix}. \tag{5}$$

Equations (4), (5) contain more dependent variables than equations; hence closure models for the Reynolds stress tensor ($\overline{\rho u_i' u_j'}$) and the turbulent heat flux vector ($\overline{\rho H' u_j'} - \overline{u_i'\sigma_{ij}}$) are required. A simple algebraic shear stress model (e.g. Baldwin–Lomax) may be 'adequate' in many instances. If not, the next level of complexity appends the time-averaged two-equation TKE system to equations (4) and (5) in concert with an algebraic Reynolds stress model. For the TKE system, wherein $\rho k = \bar{\rho}\tilde{k} = \tfrac{1}{2}\overline{\rho u_i' u_i'}$, and using the Launder–Spalding[20] correlation for pressure–strain and the Daly–Harlow[26] gradient diffusion model (see also Reference 27), the additional entries in the flux vector f_j are

$$f_j^{\mathrm{a}} = \begin{pmatrix} \tilde{u}_j\overline{\rho k} + \left(C_k\overline{\rho u_i' u_j'}\,\dfrac{\tilde{k}}{\tilde{\varepsilon}} - \bar{\mu}\delta_{ij}\right)\dfrac{\partial \tilde{k}}{\partial x_i} \\ \tilde{u}_j\overline{\rho\varepsilon} + \left(C_\varepsilon\overline{\rho u_i' u_j'}\,\dfrac{\tilde{k}}{\tilde{\varepsilon}}\right)\dfrac{\partial \tilde{\varepsilon}}{\partial x_i} \end{pmatrix}. \tag{6}$$

The source term that is now added to equation (4) is

$$s = \begin{pmatrix} 0 \\ 0 \\ 0 \\ \overline{\rho u_i' u_j'}\,\dfrac{\partial \tilde{u}_i}{\partial x_j} + \bar{\rho}\tilde{\varepsilon} \\ C_\varepsilon^1\overline{\rho u_i' u_j'}\,\dfrac{\varepsilon}{\tilde{k}}\dfrac{\partial \tilde{u}_i}{\partial x_j} + C_\varepsilon^2\bar{\rho}\dfrac{\tilde{\varepsilon}^2}{\tilde{k}} \end{pmatrix} \tag{7}$$

and the isotropic dissipation function $\tilde{\varepsilon}$ is related to a turbulence length scale l_{D} as

$$\tilde{\varepsilon} \equiv C_{\mathrm{D}}\frac{\tilde{k}^{3/2}}{l_{\mathrm{D}}}. \tag{8}$$

The coefficients C_ε^a in equation (7) are model constants, standard values for which are well established for incompressible and (mildly) compressible flows.

The TLNS equation system

The 3 DNS differential equation system is now

$$\frac{\partial q}{\partial t}+\frac{\partial f_j}{\partial x_j}+s=0. \tag{9}$$

Referencing to freestream (M_∞) and the associated stagnation properties ($p_0, a_0, H_0, \gamma_0, \mu_0, k_0$) for non-dimensionalization, and deleting the overbar notation for mean flow variables, the (non-dimensional) variables in equation (9) are

$$q=\begin{pmatrix}\rho\\ \rho u_i\\ \rho H-\dfrac{p}{\gamma_0}\\ \rho k\\ \rho\varepsilon\end{pmatrix},\qquad s=\begin{pmatrix}0\\ 0\\ 0\\ -P+\varepsilon\\ \dfrac{\varepsilon}{k}(-C_\varepsilon^1 P+C_\varepsilon^2\rho\varepsilon)\end{pmatrix},\qquad f_j=\begin{pmatrix}\rho u_j\\ u_j\rho u_i+\dfrac{p}{\gamma_0}\delta_{ij}-s_{ij}\\ u_j\rho H+q_j\\ u_j\rho k+k_j\\ u_j\rho\varepsilon+\varepsilon_j\end{pmatrix}. \tag{10}$$

Equations (9), (10) are closed with the following (non-dimensional) equations:

$$\begin{aligned}
p&=\gamma_0(1-\gamma^{-1})\left(\frac{1}{\gamma_0-1}\overline{\rho H}-\frac{1}{2}\overline{\rho u_i}\tilde{u}_i\right),\\
s_{ij}&=\overline{\sigma_{ij}}-\overline{\rho u_i' u_j'},\\
q_j&=\overline{q_j}+\overline{\rho u_j' H'}-\overline{u_i'\sigma_{ij}}-(\gamma_0-1)\tilde{u}_i\overline{\sigma_{ij}},\\
k_j&=\left(C_k\overline{\rho u_i' u_j'}\frac{\tilde{k}}{\tilde{\varepsilon}}-\frac{\bar{\mu}}{Re}\delta_{ij}\right)\frac{\partial\tilde{k}}{\partial x_i},\\
\varepsilon_j&=\left(C_\varepsilon\overline{\rho u_i' u_j'}\frac{\tilde{k}}{\tilde{\varepsilon}}\right)\frac{\partial\tilde{\varepsilon}}{\partial x_i},
\end{aligned} \tag{11}$$

with

$$\begin{aligned}
\overline{\sigma_{ij}}&=\frac{\bar{\mu}}{Re}\left(\frac{\partial\bar{u}_i}{\partial x_j}+\frac{\partial\bar{u}_j}{\partial x_i}-\frac{2}{3}\frac{\partial\bar{u}_k}{\partial x_k}\delta_{ij}\right),\\
\overline{q_j}&=-\frac{1}{RePr}k\frac{\overline{\partial T}}{\partial x_i},
\end{aligned} \tag{12}$$

where $Re=\rho_0 a_0 L/\mu_0$, $Pr=\gamma_0\mu_0 R/(\gamma_0-1)k_0$ and L is a convenient length scale. The Reynolds stress tensor and heat flux vector closure equations (equation (3)) are unchanged in the non-dimensional form.

The key TLNS algorithm step is to recast equation (9) using a (body-fitted) co-ordinate transformation $x_i=(x,y,z)\rightarrow(\xi,\eta,\zeta)$ that nominally aligns the ξ co-ordinate with the principal flow direction. For non-time-varying boundaries, the form is

$$\xi = \xi(x, y, z), \quad \eta = \eta(x, y, z), \quad \zeta = \zeta(x, y, z), \tag{13}$$

whereupon equation (9) becomes

$$\frac{\partial q}{\partial t} + \frac{\partial (E - E_v)}{\partial \xi} + \frac{\partial (F - F_v)}{\partial \eta} + \frac{\partial (G - G_v)}{\partial \zeta} + s = 0. \tag{14}$$

The non-viscous (Euler) elements of equation (14) are

$$E = \frac{1}{J}\begin{pmatrix} \rho U \\ \rho u U + \xi_x \gamma_0^{-1} p \\ \rho v U + \xi_y \gamma_0^{-1} p \\ \rho w U + \xi_z \gamma_0^{-1} p \\ \rho H U \\ \rho k U \\ \rho \varepsilon U \end{pmatrix}, \quad F = \frac{1}{J}\begin{pmatrix} \rho V \\ \rho u V + \eta_x \gamma_0^{-1} p \\ \rho v V + \eta_y \gamma_0^{-1} p \\ \rho w V + \eta_z \gamma_0^{-1} p \\ \rho H V \\ \rho k V \\ \rho \varepsilon V \end{pmatrix},$$

$$G = \frac{1}{J}\begin{pmatrix} \rho W \\ \rho u W + \zeta_x \gamma_0^{-1} p \\ \rho v W + \zeta_y \gamma_0^{-1} p \\ \rho w W + \zeta_z \gamma_0^{-1} p \\ \rho H W \\ \rho k W \\ \rho \varepsilon W \end{pmatrix}, \quad s = \begin{pmatrix} 0 \\ 0 \\ 0 \\ 0 \\ 0 \\ -P + \rho\varepsilon \\ \frac{\varepsilon}{k}(-C_\varepsilon^1 P + C_\varepsilon^2 \rho\varepsilon) \end{pmatrix}, \tag{15}$$

where J is the Jacobian of equation (13), and the contravariant velocity (**U**) scalar components parallel to the (ξ, η, ζ) co-ordinate system are

$$\begin{aligned} U &= \xi_x u + \xi_y v + \xi_z w, \\ V &= \eta_x u + \eta_y v + \eta_z w, \\ W &= \zeta_x u + \zeta_y v + \zeta_z w. \end{aligned} \tag{16}$$

The diffusive (viscous/turbulent) elements of equation (14) are

$$E_v = \frac{1}{J}\begin{pmatrix} 0 \\ \xi_x s_{xx} + \xi_y s_{xy} + \xi_z s_{xz} \\ \xi_x s_{yx} + \xi_y s_{yy} + \xi_z s_{yz} \\ \xi_x s_{zx} + \xi_y s_{zy} + \xi_z s_{zz} \\ \xi_x q_x + \xi_y q_y + \xi_z q_z \\ \xi_x k_x + \xi_y k_y + \xi_z k_z \\ \xi_x \varepsilon_x + \xi_y \varepsilon_y + \xi_z \varepsilon_z \end{pmatrix},$$

$$F_v = \frac{1}{J}\begin{pmatrix} 0 \\ \eta_x s_{xx} + \eta_y s_{xy} + \eta_z s_{xz} \\ \eta_x s_{yx} + \eta_y s_{yy} + \eta_z s_{yz} \\ \eta_x s_{zx} + \eta_y s_{zy} + \eta_z s_{zz} \\ \eta_x q_x + \eta_y q_y + \eta_z q_z \\ \eta_x k_x + \eta_y k_y + \eta_z k_z \\ \eta_x \varepsilon_x + \eta_y \varepsilon_y + \eta_z \varepsilon_z \end{pmatrix},$$

$$G_v = \frac{1}{J}\begin{pmatrix} 0 \\ \zeta_x s_{xx} + \zeta_y s_{xy} + \zeta_z s_{xz} \\ \zeta_x s_{yx} + \zeta_y s_{yy} + \zeta_z s_{yz} \\ \zeta_x s_{zx} + \zeta_y s_{zy} + \zeta_z s_{zz} \\ \zeta_x q_x + \zeta_y q_y + \zeta_z q_z \\ \zeta_x k_x + \zeta_y k_y + \zeta_z k_z \\ \zeta_x \varepsilon_x + \zeta_y \varepsilon_y + \zeta_z \varepsilon_z \end{pmatrix}. \tag{17}$$

Deletion of the terms in E_v, F_v and G_v involving ξ derivatives yields the TLNS simplification to the 3 DNS equation system, whereupon the notation E_v^*, F_v^* and G_v^* is usually invoked. By the elimination of these axial diffusion terms, the steady TLNS equations exhibit an initial-value character in the ξ (downstream) co-ordinate direction. However, as mentioned, the mathematical inconsistency associated with direct forward marching of the viscous TLNS equations is the departure solution. The necessary condition for suppression of the departure solution is that only the fraction ω of the local computed axial pressure gradient can be imposed in the subsonic flow regions of a TLNS solution. The remaining fraction $1-\omega$ must be replaced by the axial pressure gradient computed external to the sonic line, and

$$\omega = \omega(M_\xi) < \frac{\gamma M_\xi^2}{1+(\gamma-1)M_\xi^2}, \tag{18}$$

where M_ξ is the local axial streamwise Mach number. Applying this criteria for computing the axial pressure gradient in E, equation (15) yields p replaced by p^*.

The TLNS equation system, equations (14)–(17), is an initial-boundary-value specification. The boundary surfaces encountered include solid (and porous) aerodynamic surfaces and far-field and symmetry planes. For a non-porous surface all components of the contravariant velocity field (U, V, W) vanish, while if the surface is porous (for cooling) the corresponding normal component (V or W) takes a prescribed distribution. A wall heat recovery specification for enthalpy involves a non-homogeneous Neumann boundary condition on the normal derivative which vanishes for an adiabatic wall. For the viscous sublayer boundary layer assumption, the normal pressure gradient vanishes.

The wall boundary condition for the TKE closure is $k = 0 = \varepsilon$ for a sufficiently refined grid. For attached flows this resolution may not be necessary, permitting use of wall function relations. Using the 'law of the wall' analysis,[28] the slip-wall boundary condition for the contravariant velocity component U is

$$\frac{U}{u_\tau} = \frac{1}{\kappa}\ln(y^+ \bar{E}) \tag{19}$$

in the region $30 \leqslant y^+ \leqslant 100$, where u_τ is the friction velocity, κ is the Karman constant, $\bar{E}$ is a surface roughness parameter and $y^+ = yu_\tau/\nu$. In this region, assuming $P \approx \varepsilon$, where $P = u_\tau^2 \partial U/\partial y$, also

$$\tilde{k} \approx u_\tau^2/\sqrt{C_\nu}, \quad \tilde{\varepsilon} \approx u_\tau^3/\kappa y. \tag{20}$$

TAYLOR WEAK STATEMENT FINITE ELEMENT ALGORITHM

The finite element solution algorithm for the TLNS equation system, equations (14)–(18), is derived using the Taylor weak statement developed by Baker and Kim.[29] Since equation (14) defines an evolution statement, there must exist the Taylor series

$$q^{n+1} = q^n + \Delta t q_t^n + \tfrac{1}{2}\Delta t^2 q_{tt}^n + \tfrac{1}{6}\Delta t^3 q_{ttt}^n + \ldots, \tag{21}$$

where subscript 't' denotes order of temporal derivative at t_n and $t_{n+1} = t_n + \Delta t$. Equation (14)

permits restatement of the first term in equation (21) as

$$q_t = -\frac{\partial f_j}{\partial x_j} - s = -\frac{\partial f_j}{\partial q}\frac{\partial q}{\partial x_j} - s \equiv -\bar{A}_j q_j - s \tag{22}$$

which defines $\tilde{A}_j$, the Jacobian of the TLNS flux vector f_j. For the TLNS system written in the co-ordinate transformation (equation (14)) with unit vector **e**, we have

$$\begin{aligned}\bar{A}_j &= \frac{\partial(E-E_v)}{\partial q}\hat{e}_1 + \frac{\partial(F-F_v)}{\partial q}\hat{e}_2 + \frac{\partial(G-G_v)}{\partial q}\hat{e}_3 \\ &\equiv A_j - \frac{\partial E_v}{\partial q}\hat{e}_1 + \frac{\partial F_v}{\partial q}\hat{e}_2 + \frac{\partial G_v}{\partial q}\hat{e}_3 .\end{aligned} \tag{23}$$

Equation (23) defines A_j as the Jacobian of the 'Euler' flux vector, i.e. that component associated with non-viscous and non-dissipative mechanisms. Using equation (14), therefore,

$$A_j = \begin{bmatrix} U_j, & 0, & 0, & 0, & 0 \\ U_i U_j\left(\frac{\gamma-1}{2\gamma}\delta_{ij} - 1\right), & U_j\left(1+\frac{\delta_{ij}}{\gamma}\right), & 0, & 0, & 0 \\ 0, & 1-1/\gamma, & U_j, & 0, & 0 \\ 0, & 0, & 0, & U_j, & 0 \\ 0, & 0, & 0, & 0, & U_j \end{bmatrix}, \tag{24}$$

where U_j are the scalar components of **U** in the η-coordinate system, i.e. (U, V, W), equation (16).

Following Baker and Kim,[29] the second derivative term in equation (21) is approximated as

$$\begin{aligned} q_{tt} \simeq \left(\frac{\partial f_j}{\partial x_j}\right)_t &= \frac{\partial}{\partial x_j}\left(\frac{\partial f_j}{\partial t}\right) = \frac{\partial}{\partial x_j}\left(\frac{\partial f_j}{\partial q} q_t\right) = \frac{\partial}{\partial x_j}\left(-\frac{\partial f_j \partial f_k}{\partial q \partial x_k}\right) \\ &\equiv \frac{\partial}{\partial x_j}\left(\bar{\alpha} A_j q_t + \bar{\beta} A_j A_k \frac{\partial q}{\partial x_k}\right), \end{aligned} \tag{25}$$

where $\bar{\alpha}$ and $\bar{\beta}$ are arbitrary parameters forming a convex sum. The third derivative term in equation (21) is similarly evaluated, yielding

$$\begin{aligned} q_{ttt} \simeq \ldots \equiv \frac{\partial}{\partial x_j}\Bigg[&\bar{\gamma}\left(A_j A_k \frac{\partial}{\partial x_k} + \frac{\partial}{\partial x_k}(A_j A_k)\right) q_t \\ &+ \bar{\mu}\left(A_j A_k \frac{\partial}{\partial x_k} + \frac{\partial}{\partial x_k}(A_j A_k)\right) A_l \frac{\partial q}{\partial x_l}\Bigg]. \end{aligned} \tag{26}$$

Combining equations (21)–(26), taking the limit as $\Delta t \to 0$, but retaining the two higher-order terms yields the augmented (for discrete approximation) TLNS equation system as

$$\begin{aligned} L_w(q) \equiv q_t &- \frac{\partial}{\partial x_j}\left(\alpha A_j q_t + \gamma \Delta t\, A_j A_k \frac{\partial q_t}{\partial x_k}\right) + s \\ &+ \bar{A}_j \frac{\partial q}{\partial x_j} - \Delta t \frac{\partial}{\partial x_j}\left(\beta A_j A_k \frac{\partial q}{\partial x_k} + \mu \Delta t\, A_j A_k A_l \frac{\partial^2 q}{\partial x_l x_k}\right) + \ldots = 0, \end{aligned} \tag{27}$$

where $\alpha, \beta, \gamma, \mu$(without overbars) are defined to include the constants of the original Taylor series,

equation (21). Equation (27) is identical to the TLNS conservation law statement in the limit; in the CFD sequel, $\Delta t \neq 0$, whereupon combinations and simplifications of the additional terms in equation (27) contain the structure of a variety of numerical dissipation mechanisms.

Defining the Taylor weak statement (TWS) finite element algorithm for equation (27) involves application of the classical procedure. From $S^h \subset H^m, m \geqslant 1$, select the subspace $\psi_j(\eta)$ to construct the semi-discrete approximation as

$$q(\boldsymbol{\eta}, t) \approx q^h(\boldsymbol{\eta}, t) \equiv \sum_j Q_j(t)\psi_j(\boldsymbol{\eta}) \equiv \bigcup_e \{N_k(\boldsymbol{\eta})\}^{\mathrm{T}}\{Q(t)\}_e. \tag{28}$$

The Galerkin definition for test space is used; hence, for $v^h \in V^h \subset S^h$ an arbitrary test space, the TWS finite element algorithm requires

$$\int_\Omega v^h(\boldsymbol{\eta}) L_{\mathrm{w}}(q^h)\,\mathrm{d}\mathbf{x} \equiv \sum_e \int_{\Omega_e} \{N_k(\boldsymbol{\eta})\} L_{\mathrm{w}}(q^h)\,\mathrm{d}\mathbf{x} \equiv \{\mathbf{0}\}. \tag{29}$$

Equation (29) is a matrix ordinary differential equation written on the time derivative of the semi-discrete solution expansion coefficient set $\{Q\}$, equation (28). For equation (14), the specific form is

$$\begin{aligned} L(\{Q\}) = {} & M\,\mathrm{d}\{Q\}/\mathrm{d}t + \{E^h - E_{\mathrm{v}}^h\}_\xi + \{F^h - F_{\mathrm{v}}^h\}_\eta + \{G^h - G_{\mathrm{v}}^h\}_\zeta + \{S^h\} \\ & - \Delta t(\{E^h(\alpha, \beta, \mathbf{A})\}_{\xi\eta} + \{F^h(\alpha, \beta, \mathbf{A})\}_{\eta\eta} + \{G^h(\alpha, \beta, \mathbf{A})\}_{\zeta\eta}) \\ & - \Delta t^2(\{E^h(\alpha, \beta, \mathbf{A}^2)\}_{\xi\eta} + \ldots)_\eta. \end{aligned} \tag{30}$$

The first line of terms in equation (30) constitutes the conventional (Bubnov–Galerkin) finite element weak statement for the TLNS system, equation (14), including all viscous and source terms. The second and third groups of terms constitute the options for embedding of required stability mechanisms according to the definitions for $\alpha, \beta, \gamma, \mu$ and $\mathbf{A}$ (with scalar components A_j in the $\boldsymbol{\eta}$ co-ordinate system).

The TWS fully discrete solution algorithm is completed by defining a linear algebra statement using equation (30). For notational simplicity, the matrix functional form of equation (30) is

$$M(\alpha, \gamma)\mathrm{d}\{Q\}/\mathrm{d}t + \{R(\{Q\}, \beta, \mu, \{S\}, \mathbf{A}, \Delta t)\} = \{\mathbf{0}\} \tag{31}$$

and the specific construction for $M(\cdot)$ and $\{R(\cdot)\}$ depends on the choice for the trial space ($\{N_k\}$) and the TWS parameters. Once selected, equation (31) is employed to evaluate the time derivative of the discrete Taylor series

$$\{Q\}_{n+1} = \{Q\}_n + \Delta t \mathrm{d}\{Q\}/\mathrm{d}t|_{n+\theta} + \ldots, \tag{32}$$

where $\frac{1}{2} \leqslant \theta \leqslant 1$ yields the (required) implicit algorithm. Substituting equation (31) and rearranging terms produces the TWS algorithm algebra statement

$$\{F\} = M\{\Delta Q\} + \Delta t(\theta\{R\}_{n+1} + (1-\theta)\{R\}_n) = \{\mathbf{0}\}, \tag{33}$$

where $\{\Delta Q\} \equiv \{Q\}_{n+1} - \{Q\}_n$ and subscript $(n+1, n)$ denotes evaluation at the corresponding time level. Linearizing at t_n produces the TWS linear algebra statement in delta form:

$$\left[M + \theta\Delta t \frac{\partial\{R\}}{\partial\{Q\}}\right]\{\Delta Q\} = -\Delta t\{R\}_n. \tag{34}$$

The form of equation (34) is ideally suited to determination of time-accurate unsteady and/or steady state solutions, the principal goal. The steady state solution has converged when $\{R(\cdot)\} \to \{\mathbf{0}\}$ for arbitrary Δt, hence depends only on the TWS parameters β, μ and $\mathbf{A}$. The

rate of approach to steady state depends on $\alpha, \beta, \gamma, \mu, \Delta t$ and θ, and in the limit $\Delta t \to \infty$ equation (34) is a Newton algorithm.

Equation (34) ultimately resides in a code, and the matrix iterative solution procedure selected is crucial to efficiency. Of the numerous candidate methods, a tensor matrix product factorization of the Jacobian, coupled with a downstream (ξ) factor to embed direct space marching, appears most appropriate.[30-32] The Jacobian of the numerical linear algebra procedure replaces equation (34) by the factored form

$$J \equiv \left[M + \theta \Delta t \frac{\partial \{R\}}{\partial \{Q\}} \right] \simeq J_\xi \otimes J_\eta \otimes J_\zeta . \tag{35}$$

The factors J_η and J_ζ, spanning the plane transverse to the principal flow direction, are classical constructions; i.e.

$$J_\eta \equiv M_\eta + \theta \Delta t \frac{\partial \{R\}_\eta}{\partial \{Q\}}, \quad J_\zeta \equiv M_\zeta + \theta \Delta t \frac{\partial \{R\}_\zeta}{\partial \{Q\}}, \tag{36}$$

each of which is block $(2k+1)$ diagonal, where k is the completeness degree of the finite element basis $\{N_k\}$. The principal flow direction factor J_ξ is the 'upwind' construction J_ξ^{u} dependent upon the pressure interaction (TLNS) algorithm selected, of the form

$$J_\xi^{\mathrm{u}} \equiv \left[M_\xi + \theta \Delta t \frac{\partial \{R\}_\xi}{\partial \{Q\}} \right]^{\mathrm{u}} . \tag{37}$$

THEORETICAL ANALYSIS

Convergence, asymptotic error estimates

The statistically averaged Navier–Stokes equation system, equations (9)–(12), is incompletely elliptic, partially parabolic or hyperbolic dependent upon the definition of the stress tensor and constitutive closure relations, equations (11)–(12). A rigorous asymptotic error estimate for the TWS algorithm is not published. However, Galerkin finite element error estimates are available for simplified model equations of the appropriate form.[33] For a (steady state) regular elliptic boundary value problem, and denoting the discrete approximation error as $e^h \equiv q - q^h$, the asymptotic error estimate is (Reference 33, equation (8.80))

$$\| e^h \|_{H^1(\Omega)} \leqslant C(h_{\mathrm{m}}^{\gamma_1} \| f \|_{H^r(\Omega)} + h_{\mathrm{m}}^{\gamma_2} \| g \|_{H^p(\partial\Omega)}). \tag{38}$$

In equation (38), $\| \cdot \|_{H(\cdot)}$ is the Sobolev norm defined on the solution domain (Ω) and its boundary ($\partial\Omega$), f and g are the corresponding Dirichlet data, $r \geqslant 0$ is a measure of solution differentiability and $p \geqslant \frac{1}{2}$. For sufficiently small h, C is a constant independent of h, h_{m} is the extremum mesh measure, $\gamma_1 = \min(k, r+1)$ while $\gamma_2 = \min(k, \min(p+\frac{1}{2}))$, where k is the smallest complete degree of the basis, equation (28).

For a linear parabolic initial-value problem, the error estimate at time $t = n\Delta t$ is of the form (Reference 33, equation (9.66)).

$$\| e^h(\cdot, n\Delta t) \|_{H^1(\Omega)} \leqslant C_1 h_{\mathrm{m}}^k \| q(n\Delta t) \|_{H^{k+1}(\Omega)} + C_2 \Delta t \| Q_0 \|_{H^1(\Omega)}, \tag{39}$$

where Δt is the time step, Q_0 is the interpolation of $q(x, t=0)$ onto the nodes of the mesh and C_1 and C_2 are constants independent of h for sufficiently small h. The form of equation (39) is augmented, for a smooth solution to a linear hyperbolic equation (Reference 33, equation (9.103)), as

$$\| e^h(\cdot, n\Delta t)\|_{H^1(\Omega)} \leqslant C_1 h_m^{k+1} \| q \|_{H^{k+1}(\Omega)} + C_2 \Delta t \| Q_0 \|_{H^1(\Omega)} + C_3 h^k \int_0^{n\Delta t} \| q \|_{H^{k+1}(\Omega)} dt . \tag{40}$$

Note in particular that, for sufficiently small h and Δt, convergence is dominated by the third term in equation (40), which involves the evolution of the true solution over the time interval. For non-smooth solutions to a hyperbolic equation, the exact solution will at most exist in $\| \cdot \|_{H^0(\Omega)}$ (or $\| \cdot \|_{L^1}$). While no error estimates are published, even for a model problem, viewing equations (38)–(40) one might anticipate the form to be

$$\| e^h(\cdot, n\Delta t)\|_{H^0(\Omega)} \leqslant C h_m^p \| q \|_{H^0(\Omega)} + \ldots . \tag{41}$$

A corresponding expression would exist in $\| \cdot \|_{L^1}$ and in either case (hopefully) $p > 0$.

Stability, dispersion and dissipation

The TWS finite element algorithm, equations (27)–(29), is specifically formulated to engender stability mechanisms dependent upon the choices for $\alpha, \beta, \gamma, \mu, \theta$ and A_j, a requirement amply verified for any (all) Navier–Stokes approximate solution procedures. Baker and Kim[29] develop the TWS theoretical analysis for a scalar linear hyperbolic/parabolic equation. For the restriction to a uniform mesh and the $k = 1$ basis, the TWS algorithm numerical linear algebra statement, equation (34), can be equivalently stated in terms of the central finite difference operators Δ_0 and δ^2 and the first-order upwind difference operator $\delta^2 \Delta_\pm$ as

$$[1 + \alpha_A \Delta_0 + (\tfrac{1}{6} - \alpha_B)\delta^2 + \alpha_C \delta^2 \Delta_\pm] \Delta Q_j^{n+1} = -[c\Delta_0 - c\alpha_D \delta^2 + c\alpha_E \delta^2 \Delta_\pm] Q_j^n . \tag{42}$$

In equation (42), $\Delta Q_j^{n+1} \equiv Q_j^{n+1} - Q_j^n$ and θ and the TWS parameters (recall equation (27)) are now combined within the definitions

$$\begin{aligned} \alpha_A &\equiv c(\theta - \bar{\alpha}/2 - \bar{\gamma}\Delta t a_x/3), \\ \alpha_B &\equiv c^2[\bar{\gamma}/6 + \theta(\bar{\beta}/2 + \bar{\mu}\Delta t a_x/3)] \\ \alpha_C &\equiv \theta c^3 \bar{\mu}/6 , \\ \alpha_D &\equiv c(\bar{\beta}/2 + \bar{\mu}\Delta t a_x/3), \\ \alpha_E &\equiv c^2 \bar{\mu}/6 , \end{aligned} \tag{43}$$

where $c \equiv a\Delta t/\Delta x$ is the (element) Courant number and $a = \partial f/\partial q$ is the (scalar Euler) flux vector Jacobian.

The typical term in the Fourier expansion of the exact inviscid solution is

$$q(x,t) = V \exp[i\omega(x - at)], \tag{44}$$

where $\omega = 2\pi/\lambda$ is the wave number of the mode of wavelength λ and $i = \sqrt{-1}$. For the semi-discrete approximate solution of similar form, one has on a uniform mesh of measure Δx,

$$q^h(j\Delta x, t) = V \exp[i\omega(j\Delta x - \bar{\bar{\gamma}} t)], \tag{45}$$

where $\bar{\bar{\gamma}} \equiv \bar{\bar{\beta}} + i\bar{\bar{\delta}}$ contains the dispersion and dissipation (error) components. The amplification factor g for the fully discrete solution is determined from

$$q_\Delta(j\Delta x, t + \Delta t) = g q^h(j\Delta x, t). \tag{46}$$

Substituting, from equations (42) and (46), one obtains the solution

$$g = 1 - \frac{c(\Delta_0 - \alpha_D\delta^2 + \alpha_E\delta^2\Delta_{\mp})Q_j}{[1 + \alpha_A\Delta_0 + (\frac{1}{6} - \alpha_B)\delta^2 + \alpha_C\delta^2\Delta_{\mp}]Q_j} \cdot \tag{47}$$

Using well known identities for the operators in equation (47),[29] the following estimates for the fully discrete solution dissipation error $\omega(\Delta t)\bar{\bar{\delta}}$ and phase dispersion error $\omega\Delta t(a - \bar{\bar{\beta}})$ are readily established as

$$(\omega\Delta t)\bar{\bar{\delta}} = c\left[m^2\left(\frac{c}{2} - \alpha_1\right) + m^4\left(-\frac{c^3}{8} + \alpha_1 c^2/2 - (\beta_2 - \beta)c + (\beta_1 - \beta\alpha_1)\right) + m^6(\cdot) + \cdots \right], \tag{48}$$

$$(\omega\Delta t)(a - \bar{\bar{\beta}}) = c\left[m^3\left(\frac{c^2}{3} - \alpha_1 c + (\beta_2 - \beta)\right) + m^5\left(-\frac{c^4}{30} + \frac{\alpha_1 c^3}{6} - \frac{(\beta_2 - \beta)c^2}{2} + (\beta_1 - \beta\alpha_1)c - [\gamma_2 - \gamma - \beta(\beta_2 - \beta)]\right) + m^7(\cdot) + \cdots \right]. \tag{49}$$

The coefficients $\alpha_1, \beta_1, \beta_2, \ldots$ are functions of $\alpha_A, \alpha_B, \ldots, c, \theta$ (equation (43)) and the sign of the Jacobian (sgn a), and both error functions are series expansions in the element measure $m \equiv \omega\Delta x$. Upon definition of the TWS theory parameters, equations (48), (49) quantify the stability mechanisms of the corresponding algorithm.

DISCUSSION AND RESULTS

TWS algorithm stability characterization

The classification of CFD algorithms on the basis of stability mechanisms for application to the inviscid form of equation (9) (equation (1)) can be organized into three general categories:

(1) those with dissipation mechanisms independent of Courant number (donor cell type);
(2) those with dissipation mechanisms dependent upon Courant number (Lax–Wendroff type);
(3) those of either type with independently defined parameters.

A specific (published) algorithm in any of the three categories can be either implicit or explicit. Table I (from Reference 29) summarizes the categorical distinctions of 16 algorithms according to the definitions of equations (42), (43).

As the base-line case, the conventional (Bubnov–) Galerkin (BG) algorithm is specified by $\alpha_A = c\theta, \bar{\alpha} = 0 = \bar{\beta} = \bar{\gamma} = \bar{\mu}$, yielding for equations (48), (49)

$$\omega\Delta t(\bar{\bar{\delta}}) = c[c(\tfrac{1}{2} - \theta)m^2 + c^3(-\tfrac{1}{8} + \tfrac{1}{2}\theta - \theta^2 + \theta^3)m^4 + \ldots], \tag{50a}$$

$$\omega\Delta t(a - \bar{\bar{\beta}}) = c[c^2(\tfrac{1}{3} - \theta + \theta^2)m^3 + \ldots]. \tag{50b}$$

Therefore for $\theta = 0$ the algorithm is unstable ($\bar{\bar{\delta}} > 0$), for $\theta = \frac{1}{2}$ dissipation is $O(m^6)$ and decreases to $O(m^2)$ for $\theta = 1$. Phase dispersion is $O(m^3)$ independent of θ. For a linear travelling sine wave test, Figure 1(*a*) confirms relative freedom from diffusion ($\theta = \frac{1}{2}$) with large lagging phase distortion. For the non-linear stationary shock, Figure 1(*b*) fully confirms the inherent instability of BG independent of θ for the steady solution.

The explicit donor cell and Lax–Wendroff[34] finite difference (FD) algorithms form the essence of many of the more recently derived FE algorithms. Donor cell, with dissipation mechanism independent of Courant number, is obtained by the definitions $\alpha_A = 0 = \alpha_C = \alpha_E = \theta, \alpha_B = \frac{1}{6}$ (to cancel the mass matrix) and $\alpha_D \equiv (\text{sgn } a)/2$. Thus from equations (48), (49)

Table I. CFD algorithm comparisons using the Taylor weak statement construction (from Baker and Kim[29])

Methods	Eqtn ( ) ref. [ ]	θ	α_A	$(\frac{1}{6}-\alpha_B)$	α_C	$-\alpha_D$	α_E	Comments
Taylor weak statement	(32)	All	$c\left(\theta-\frac{\bar{\alpha}}{2}-\frac{\bar{\gamma}}{3}\Delta t a_x\right)$	$\frac{1}{6}-\left(c^2\frac{\bar{\gamma}}{6}+\theta\left(\frac{\bar{\beta}}{2}+\frac{\bar{\mu}}{2}\Delta t a_x\right)\right)$	$c^3\theta\frac{\bar{\mu}}{6}$	$-c\left(\frac{\bar{\beta}}{2}+\frac{\bar{\mu}}{2}\Delta t a_x\right)$	$c^2\frac{\bar{\mu}}{6}$	$\bar{\alpha},\bar{\beta},\bar{\gamma},\bar{\mu},\theta$ arbitrary
Bubnov–Galerkin	(54)	All	$c\theta$	$\frac{1}{6}$	0	0	0	$\bar{\alpha}=0=\bar{\beta}=\bar{\mu}=\gamma$
Donor cell upwind	[12]	0	0	0	0	$\frac{\operatorname{sgn} a}{2}$	0	$\lvert c\rvert\leqslant 1$
Lax–Wendroff	[13]	0	0	0	0	$-\frac{c}{2}$	0	$\lvert c\rvert\leqslant 1$
Euler Taylor–Galerkin	[9]	0	$c\bar{\theta}$	$\frac{1}{6}-\frac{c^2}{6}(1-3\bar{\theta})$	0	$-c(\frac{1}{2}-\bar{\theta})$	0	$\bar{\theta}=0$ for ETG, $\bar{\theta}=\frac{1}{2}$ for CN–TG
Euler characteristic Galerkin	[8]	0	0	$\frac{1}{6}$	0	$-\frac{c}{2}$	$\frac{c^2}{6}$	$\lvert c\rvert\leqslant 1$ for this form
Swansea Taylor–Galerkin	[21]	0	0	$\frac{1}{6}$	0	$-\frac{c}{2}$	0	$c<1/\sqrt{3}$ for stability
Wahlbin	[1]	0	$c\theta-(\operatorname{sgn} a)$	$\frac{1}{6}-c(\operatorname{sgn} a)\theta$	0	$-(\operatorname{sgn} a)$	0	
Dendy	[2]	0	$c\theta-(\operatorname{sgn} a)$	$\frac{1}{6}-c(\operatorname{sgn} a)k'\theta$	0	$-(\operatorname{sgn} a)k'$	0	$Re[\Phi,k\Phi_x]\leqslant C_1\lvert\Phi\rvert^2, k=k'\Delta x, C_1>0$
Raymond–Garder	[3]	$\frac{1}{2}$	$c\theta-(\operatorname{sgn} a)v$	$\frac{1}{6}-c(\operatorname{sgn} a)v\theta$	0	$-(\operatorname{sgn} a)v$	0	$v=1\sqrt{15}$
Penalty Galerkin	[7]	All	$c\theta-(\operatorname{sgn} a)v^i$	$\frac{1}{6}-c(\operatorname{sgn} a)v_d\theta$	0	$-(\operatorname{sgn} a)v_d$	0	$v_i, v_d\approx C_a(1/\sqrt{15}), 0\leqslant C_a\leqslant 2$ for Euler eqtns
Hughes–Brooks SUPG	[5]					$-\left(\frac{a}{2}+\frac{k}{a\Delta x}\right)$	–	Steady only, k = thermal conductivity
Euler Petrov–Galerkin	[6]	0	0	$\frac{1}{6}-\frac{1}{6}(1-v)$	0	$-\frac{(\operatorname{sgn} a)v}{2}$	0	$\lvert c\rvert\leqslant v\leqslant 1$
CN Petrov–Galerkin	[6]	$\frac{1}{2}$	$\frac{c}{2}-\frac{(\operatorname{sgn} a)v}{2}$	$\frac{1}{6}-\frac{v}{2}\left((\operatorname{sgn} a)\frac{c}{2}-\frac{1}{6}\right)$	0	$-\frac{(\operatorname{sgn} a)v}{2}$	0	$\lvert c\rvert\leqslant v\leqslant 1$
Warming–Beam–explicit	[23]	0	0	0	0	$-\frac{c}{2}$	$\frac{c(1-c)}{2}$	$\lvert c\rvert\leqslant 1, a>0$
van Leer (MUSCL)	[24]	1	$c\theta$	$-c(\operatorname{sgn} a)\frac{\theta}{2}$	0	0	$-\frac{1}{2}$	Simple flux limiter ($\Phi\pm\equiv 1$)
Hughes–Mallet	[25]	0	$-\frac{l(\operatorname{sgn} a)}{2}$	$\frac{1}{6}+\frac{1}{12}$	0	$-\frac{(\operatorname{sgn} a)}{2}$	0	l is flux limiter, $0\leqslant l\leqslant 1$

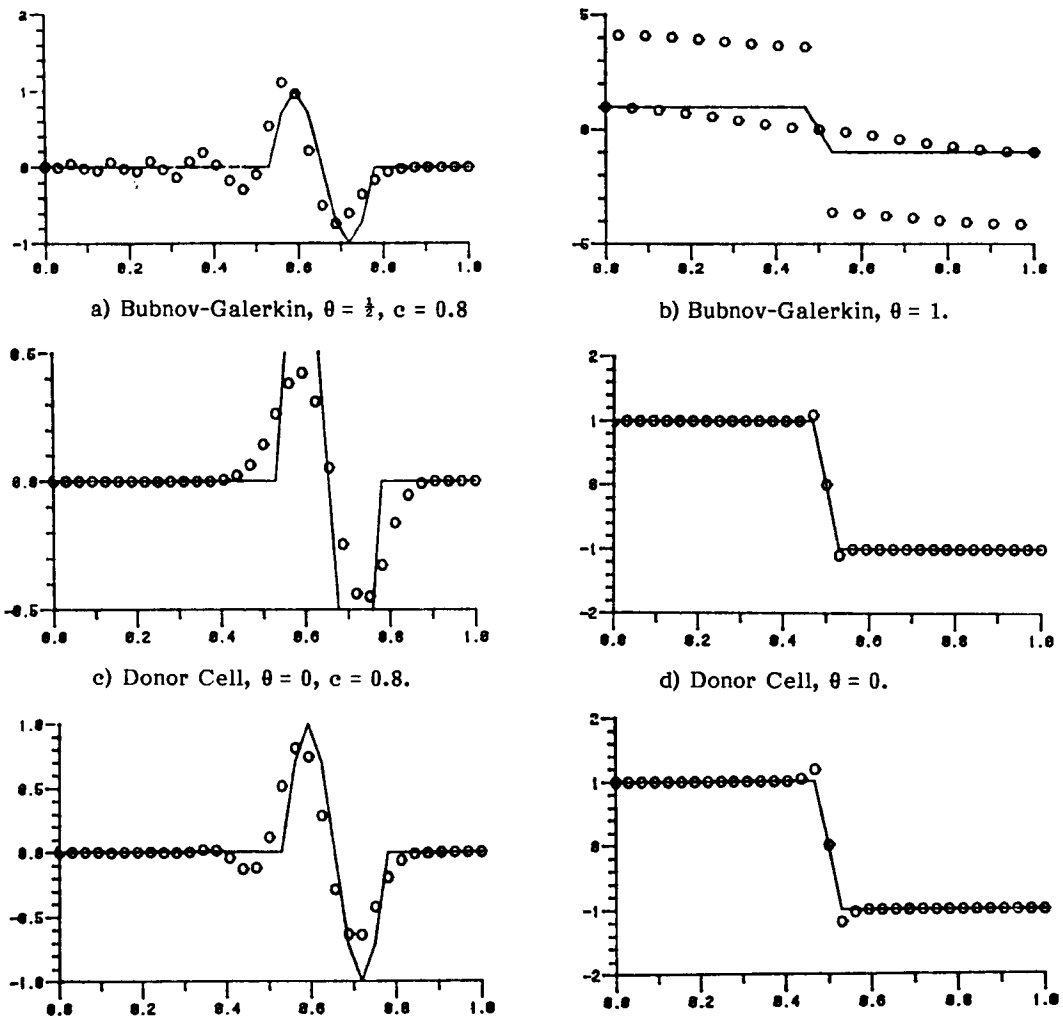

a) Bubnov-Galerkin, $\theta = \frac{1}{2}$, c = 0.8

b) Bubnov-Galerkin, $\theta = 1.$

c) Donor Cell, $\theta = 0$, c = 0.8.

d) Donor Cell, $\theta = 0.$

e) Lax-Wendroff, $\theta = 0$, c = 0.8.

f) Lax-Wendroff, $\theta = 0.$

Figure 1. CFD algorithm predictions of example inviscid test problems; (○) numerical grid point solution; (—) exact solution, linear travelling sine wave (left column), non-linear stationary shock (right column) (after Baker and Kim[29])

$$\omega \Delta t(\bar{\bar{\delta}}) = c[\tfrac{1}{2}(c-1)m^2 + \ldots], \tag{51a}$$

$$\omega \Delta t(a - \bar{\bar{\beta}}) = c[\tfrac{1}{6}(2c^2 - 3c + 1)m^3 + \ldots], \tag{51b}$$

confirming second-order dissipation, third-order phase dispersion and stability for Courant number less than unity. Rampant diffusion is evident for the travelling sine wave, Figure 1(*c*), while the stationary shock is captured with only unit Δx over- and under-shoot of modest magnitude, Figure 1(*d*). The Lax–Wendroff FD algorithm differs from donor cell only by $\alpha_D \equiv c/2$. Thus equations (48), (49) yield

$$\omega \Delta t(\bar{\bar{\delta}}) = c[\tfrac{1}{8}c(c^2 - 1)m^4 + \ldots], \tag{52a}$$

$$\omega \Delta t(a - \bar{\bar{\beta}}) = c[\tfrac{1}{6}(1 - c^2)m^3 + \ldots], \tag{52b}$$

and the distinction from donor cell is fourth-order dissipation (for $c < 1$). The large numerical diffusion is thus absent from the travelling sine wave solution, Figure 1(*e*), while a $2\Delta x$ oscillation is induced in the stationary shock, Figure 1(*f*).

Recently, several Taylor–Galerkin FE algorithms have been proposed.[35–40] These are characterized within the Taylor weak statement as explicit procedures that retain the exact form of the Taylor series, equation (25), with no parameters introduced. The Swansea Taylor–Galerkin (STG) algorithm constitutes Lax–Wendroff with a mass matrix; thus the TWS parameters are $\alpha_A = 0 = \alpha_B = \alpha_C = \alpha_E = \theta$ and $\alpha_D = c/2$. The corresponding solutions for equations (48), (49) are

$$\omega\Delta t(\bar{\bar{\delta}}) = c\left(\frac{c}{24}(3c^2 - 1)m^4 + \dots\right), \tag{53a}$$

$$\omega\Delta t(a - \bar{\bar{\beta}}) = c\left[-\frac{c}{6}m^3 + \left(\frac{7c^4}{15} - \frac{c^2}{24} + \frac{1}{180}\right)m^5 + \dots\right], \tag{53b}$$

leading to the rather severe stability constraint $c \leqslant 1/\sqrt{3}$ such that $\bar{\bar{\delta}} \leqslant 0$. Figure 2(*a*) confirms relatively large diffusion (for $c = 0.4$) and leading phase error for the travelling sine wave, and the stationary square wave oscillation, Figure 2(*b*), is somewhat larger than Lax–Wendroff, Figure 1(*f*).

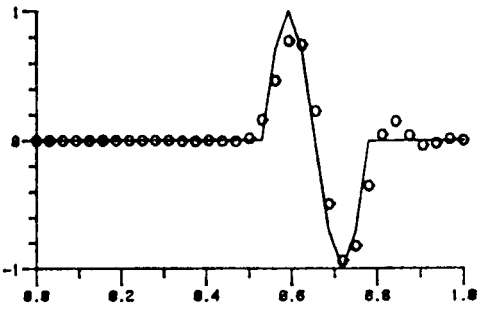

a) Swansea Taylor-Galerkin, θ = 0, c = 0.4

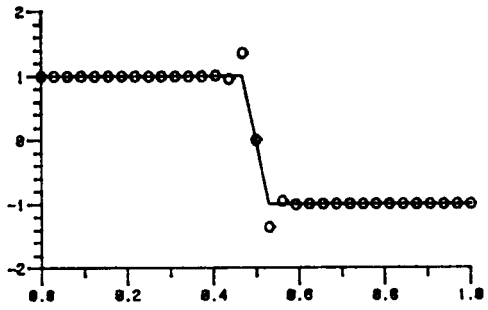

b) Swansea Taylor-Galerkin, θ= 0.

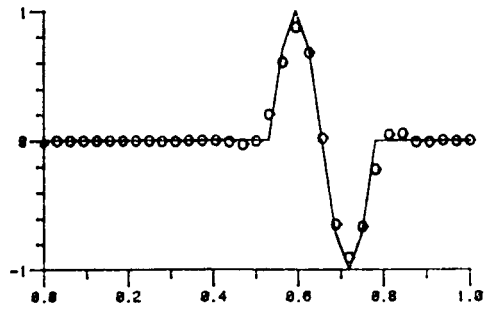

c) Euler Taylor-Galerkin, θ = 0, c = 0.8.

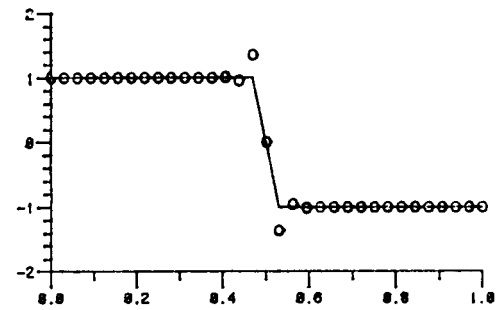

d) Euler Taylor-Galerkin, θ = 0.

Figure 2. CFD algorithm predictions of example inviscid test problems; (○) numerical grid point solution; (—) exact solution, linear travelling sine wave (left column), non-linear stationary shock (right column) (after Baker and Kim[29])

The original Euler Taylor–Galerkin (ETG) algorithm of Donea[35] constitutes the definitions $\alpha_A = 0 = \alpha_C = \alpha_E = \theta, \alpha_B = c^2/6$ and $\alpha_D = c/2$. Thus for equations (48), (49)

$$\omega \Delta t(\bar{\bar{\delta}}) = c\left(\frac{c}{24}(c^2 - 1)m^4 + \dots\right), \tag{54a}$$

$$\omega \Delta t(a - \bar{\bar{\beta}}) = c\left(\frac{1}{180}(1 - 5c^2 + 5c^4)m^5 + \dots\right), \tag{54b}$$

and like Lax–Wendroff the algorithm possesses fourth-order dissipation and is stable for $c \leqslant 1$. In distinction, it possesses fifth-order phase dispersion, hence quite accurate propagation of the travelling sine wave at $c = 0{\cdot}8$, Figure 2(*c*). Since it is Lax–Wendroff type, as with the STG algorithm, the stationary shock shows the substantial oscillation, Figure 2(*d*).

The Euler characteristic Galerkin (ECG) FE algorithm of Morton[38] constitutes an exchange in the definition of the parameters α_B and α_E, i.e. $\alpha_B = 0$ and $\alpha_E = c^2/6$, in comparison with Donea's algorithm. The subtle distinction between these is apparent in the solution of equations (48), (49), which for ECG is

$$\omega \Delta t(\bar{\bar{\delta}}) = c\left(-\frac{c}{24}(c^2 - 1)^2 m^4 + \dots\right), \tag{55a}$$

$$\omega \Delta t(a - \bar{\bar{\beta}}) = c\left[\left(\frac{1}{180} - \frac{c^2}{18} + \frac{c^3}{12} - \frac{c^4}{30}\right)m^5 + \dots\right]. \tag{55b}$$

The ECG algorithm is stable for all Courant numbers, and for $c = 1$ is sixth-order accurate as the phase dispersion coefficient also vanishes. For $c = 0{\cdot}8$, the travelling sine wave solution is indistinguishable from ETG. No results were reported for the stationary square wave.

The class of Petrov–Galerkin algorithms is characterized by introduction of an arbitrary parameter in the Taylor series, such that it is no longer exact. The algorithms of Wahlbin[41], Dendy[42] and Raymond–Garder[43] belong to this class. Hughes and Brooks[44] developed the multi-dimensional streamline–upwind Petrov–Galerkin (SUPG) formulation for steady state conservation laws with physical diffusion. Morton and Parrott[37] detail the Euler Petrov–Galerkin (EPG) formulation for the unsteady problem statement. Within the TWS, the EPG algorithm is recovered by the definitions $\alpha_A = 0 = \alpha_C = \alpha_E = \theta, \alpha_B = \frac{1}{6}(1 - \nu)$ and $\alpha_D = \nu(\operatorname{sgn} a)/2$. The theoretical characterization for equations (48), (49) thus yields

$$\omega \Delta t(\bar{\bar{\delta}}) = c\{\tfrac{1}{2}(c - \nu)m^2 + [\nu(c^2/4 + c/6 + 1/24) - \nu^2/12 - c/6 - c^3/8]m^4 + \dots\}, \tag{56a}$$

$$\omega \Delta t(a - \bar{\bar{\beta}}) = c\{[\tfrac{1}{6} + c^2/3 - \nu(3c + 1)/6]m^3 + \dots\}. \tag{56b}$$

From the original test space definition, $\nu \leqslant 1$ is required. For non-negative dissipation, the resultant (consequential) constraint is $c < \nu$. For $\nu = c$, the fourth-order diffusion term yields the stability requirement $c \leqslant \frac{1}{3}$, so there exists a rather severe time step limitation. Figure 3(*a*) confirms quite poor propagation of the travelling sine wave at $c = 0{\cdot}2$ in comparison to the STG algorithm (with similar stability limitations). The steady square wave, Figure 3(*b*), computed with $\nu = 0{\cdot}95$ appears comparable with the donor cell results as expected (compare the α_D definitions).

The Petrov–Galerkin algorithm of Raymond–Garder[43], as adapted by Baker and Soliman[45] for a FE Euler algorithm, is the only implicit form (originally developed for $\theta = \frac{1}{2}$) and corresponds to retention of the second term in the original Taylor series, equation (25), with equal weighting ($\bar{\alpha} = \bar{\beta}$). In the TWS statement, this amounts to the definitions $\alpha_A = c\theta - (\operatorname{sgn} a)\nu, \alpha_B = c\theta(\operatorname{sgn} a)\nu, \alpha_C = 0 = \alpha_E, \alpha_D = (\operatorname{sgn} a)\nu$ and θ arbitrary. The corresponding

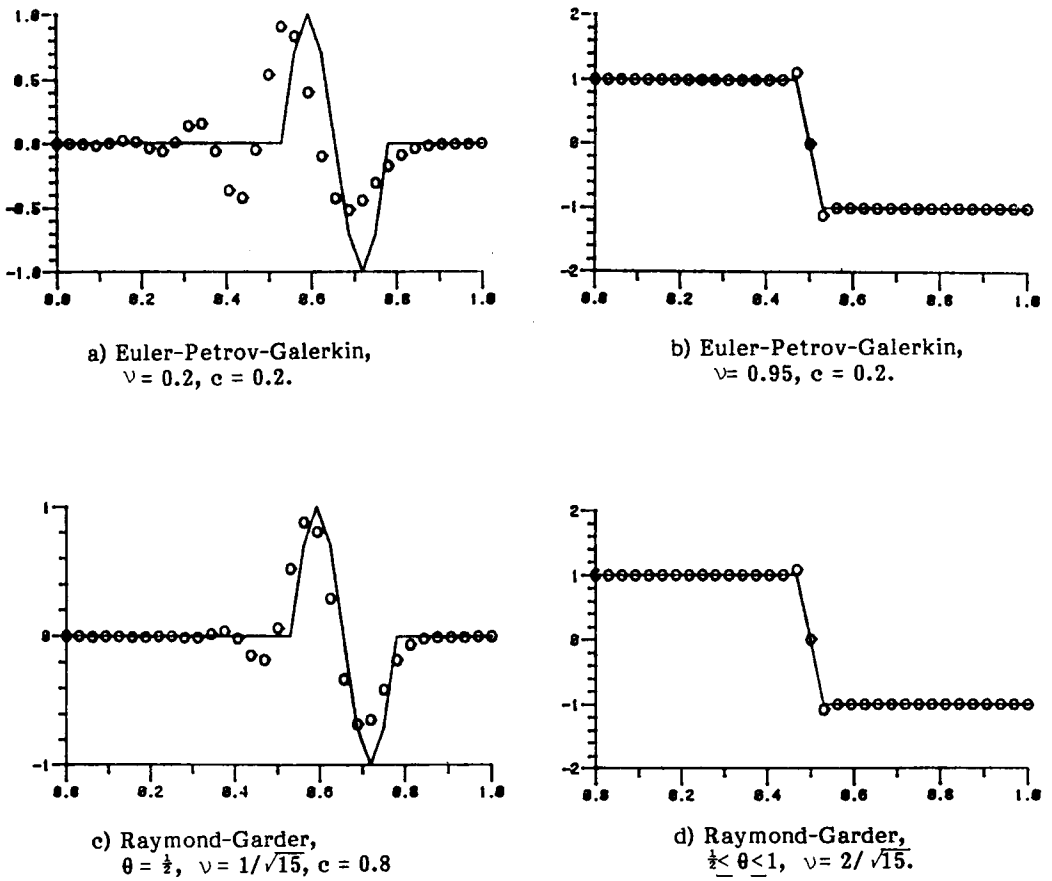

a) Euler-Petrov-Galerkin, $\nu = 0.2$, $c = 0.2$.

b) Euler-Petrov-Galerkin, $\nu = 0.95$, $c = 0.2$.

c) Raymond-Garder, $\theta = \frac{1}{2}$, $\nu = 1/\sqrt{15}$, $c = 0.8$

d) Raymond-Garder, $\frac{1}{2} \leq \theta \leq 1$, $\nu = 2/\sqrt{15}$.

Figure 3. CFD algorithm predictions of example inviscid test problems; (○) numerical grid point solution; (—) exact solution, linear travelling sine wave (left column), non-linear stationary shock (right column)(after Baker and Kim[29])

solutions for equations (48), (49) are

$$\omega \Delta t(\bar{\bar{\delta}}) = c[c(\tfrac{1}{2} - \theta)m^2 + (c^3(\theta^3 - \theta^2 + \theta/2 - \tfrac{1}{8}) - \nu/12)m^4 + \ldots], \tag{57a}$$

$$\omega \Delta t(a - \bar{\bar{\beta}}) = c[(c^2 - \theta + \tfrac{1}{3})m^3 + \ldots]. \tag{57b}$$

Comparing equations (57) and (50), the RG algorithm is identical to BG with the sole addition of a fourth-order dissipation term $\nu/12$. For $\theta \geqslant \frac{1}{2}$ and all ν, the RG algorithm is stable for all c with a third-order phase dispersion error. In the original RG analysis, $\nu = (15)^{-1/2}$ was determined 'optimal' according to a semi-discrete Fourier stability analysis. Equation (57a) confirms this conclusion erroneous, as no optimal value exists. Figure 3(*c*) confirms the RG algorithm (with $\nu = (15)^{-1/2}$) is a modest improvement over BG in propagating the sine wave at $c = 0{\cdot}8$, while the donor cell type damping is evident in the steady state square wave for $\nu = 2(15)^{-1/2}$, Figure 3(*d*).

Accuracy and convergence, supersonic flows

The Euler equations, the inviscid form of the TLNS system, provide a venue to estimate the validity and the exponent p in the asymptotic error estimate, equation (41), for non-smooth

(shocked) solutions. Baker[46] reports results for a one-dimensional (unsteady) Riemann shock tube definition. The unit interval $0 \leqslant x < 1$ is bisected; the left side initial conditions are $\rho = 0{\cdot}445$, $\rho u = 0{\cdot}311$ and $\rho e = 8{\cdot}928$, while the corresponding right side conditions are $\rho = 0{\cdot}5, \rho u = 0$ and $\rho e = 1{\cdot}4275$. This results in a shock wave propagating to the right followed by a contact discontinuity. The reported TWS algorithm statement is a variant of the Raymond–Garder definition, constituting retention of the second derivative terms in the Taylor series, equation (27). Specifically, $\bar{\gamma} = 0 = \bar{\mu}$ in equation (27) and recalling equation (24), the reported algorithm specification constitutes

$$\bar{\alpha} A_j \simeq v_0(\operatorname{sgn} A_1) \begin{bmatrix} \frac{3}{16} & 0 & 0 \\ 0 & 0 & 0 \\ 0 & 0 & \frac{1}{8} \end{bmatrix}, \tag{58a}$$

$$\bar{\beta} A_j A_k \simeq v_0(\operatorname{sgn} A_1)|u_1| \begin{bmatrix} \frac{3}{8} & 0 & 0 \\ 0 & 1 & 0 \\ 0 & 0 & \frac{1}{2} \end{bmatrix}, \tag{58b}$$

where $v_0 \equiv (15)^{-1/2}$ is the Raymond–Garder determination and the dependent variable ordering is $(\rho, \rho u, \rho e)$. The convergence study was conducted for $x = (0, 1)$ uniformly discretized into $16 \leqslant M \leqslant 256$ finite elements for the linear basis ($k = 1$, equation (28)) TWS algorithm implementation. The norms computed were H^0 and L^1, and Figure 4 graphs the resulting estimates of the semi-discrete approximation error for ρ^h, ρu^h, and p^h. The L^1 data are interpolated almost exactly by the line of unit slope, while the coarse grid inaccuracy is more evident in H^0.

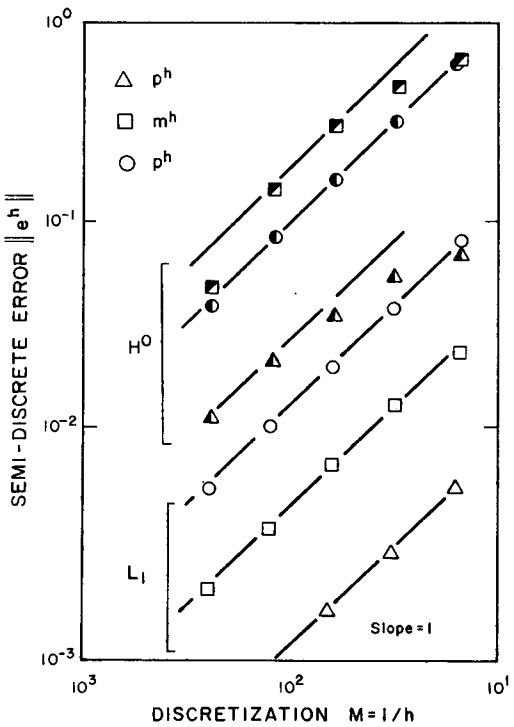

Figure 4. TWS algorithm estimation of asymptotic convergence rates; Riemann shock tube problem of Lax, $k = 1, 16 \leqslant M \leqslant 256$ (from Baker[45])

The TLNS equation system also contains the boundary layer equations as a subset. Computational tests have verified the theoretical asymptotic convergence rate, equation (39), for a non-interactive laminar 2D boundary layer solution at $M_\infty = 2{\cdot}5$. The BG algorithm is utilized and $\theta = \frac{1}{2}$ implicit solutions generated using the linear and quadratic trial (and test) spaces. Figure 5

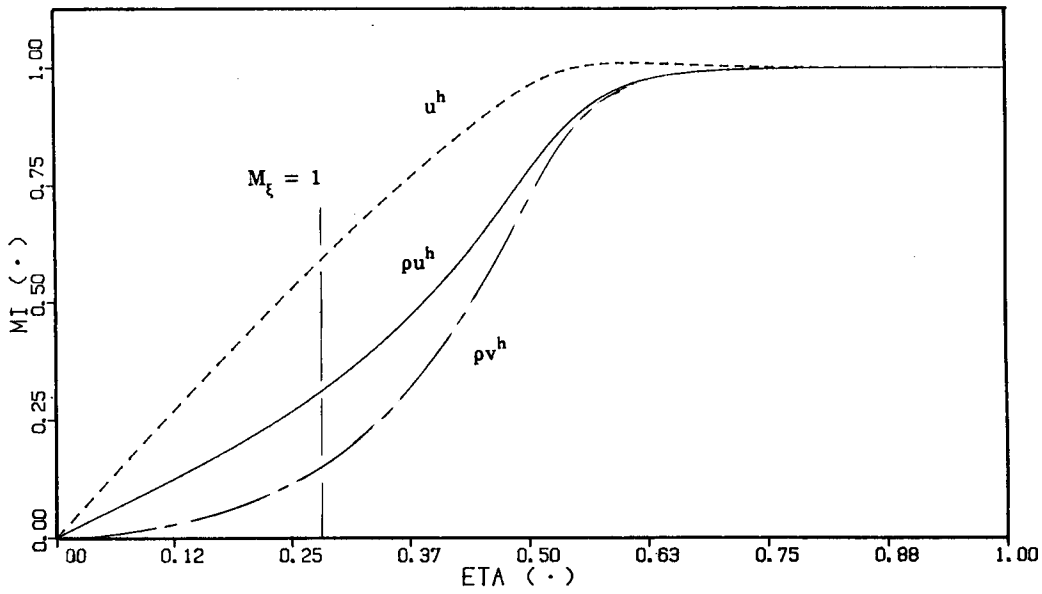

(a)

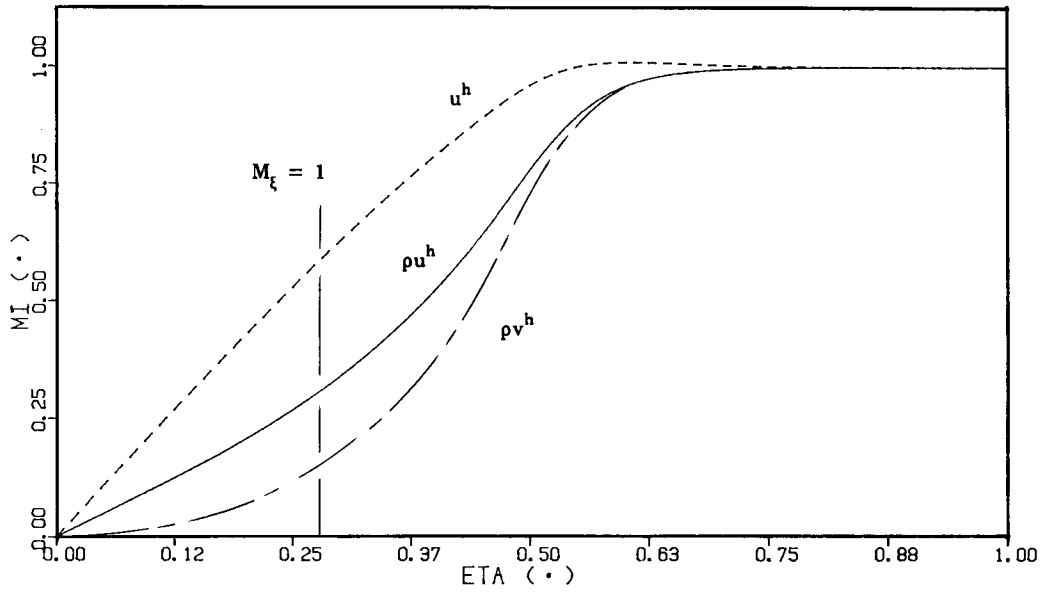

(b)

Figure 5. BG finite element algorithm prediction of supersonic viscous boundary layer velocity and momenta, $M_\infty = 2{\cdot}5$. (*a*) Linear basis ($k = 1$), $M = 128$. (*b*) Quadratic basis ($k = 2$), $M = 64$

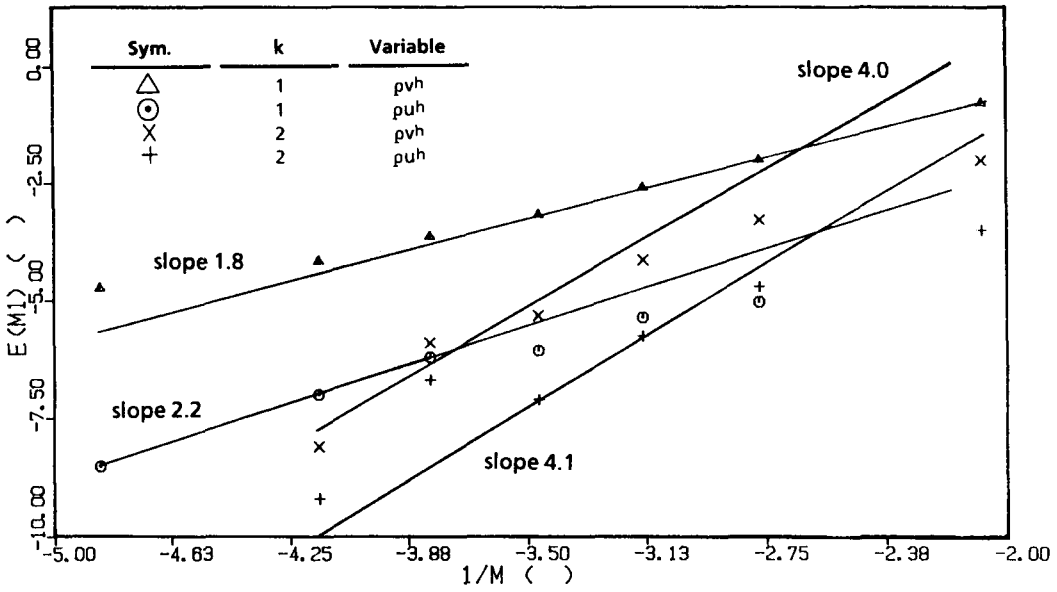

Figure 6. Convergence in energy semi-norm, BG finite element algorithm, laminar supersonic boundary layer, $M_\infty = 2{\cdot}5$, linear and quadratic basis

graphs the computed solutions for momenta and velocity for the $k = 1$, $M = 128$ discretization and a $k = 2$, $M = 64$ discretization solution. The results are visually indistinguishable and clearly illustrate essential linearity for axial velocity (u^h) over the range of the normal coordinate (η). The computed asymptotic convergence with discretization refinement for both algorithms is graphed in Figure 6. Interpolation of the numerical data agrees closely with the theoretical prediction, equation (39). The significantly improved $k = 2$ accuracy level strongly suggests that no *a priori* decision should be made regarding use of only the most elementary basis for a FE aerodynamics algorithm.

Tensor product linear algebra solution

A key algorithm aspect is the matrix iteration algorithm for the numerical linear algebra statement, equations (33), (34). The test problem is unsteady convection–diffusion of a scalar field ϕ in the two-dimensional transverse plane spanned by the η, ζ co-ordinate system. The governing equation is

$$\phi_t + \nabla\cdot(\mathbf{u}\phi) - \nabla\cdot\mathbf{k}\nabla\phi = 0 \tag{59}$$

and the BG finite element algorithm linear algebra statement is

$$[M + \theta\Delta t(U_1C_1 + U_2C_2 + KD_1 + KD_2)]\{\Delta Q\} = -\Delta t\{R\}^n, \tag{60a}$$

$$\{R\}^n = [U_1C_1 + U_2C_2 + KD_1 + KD_2]\{Q\}^n. \tag{60b}$$

The arrays U_1 and U_2 are the (contravariant) convection velocity components parallel to (η, ζ), K is the (constant) thermal conductivity and C_1, C_2, D_1 and D_2 are the corresponding convection and diffusion matrices, as constructed from discrete evaluation of the flux vectors $(E - E_v)$ and $(F - F_v)$. equation (30).

The tensor matrix product decomposition of the Jacobian of equation (60a), recall

equations (35), (36) is

$$J = J_\eta \otimes J_\zeta \equiv J_1 \otimes J_2, \tag{61}$$

where

$$J_1 = S_e(J_1)_e = S_e[M_e + \theta\Delta t(U_1 C + KD)_e], \tag{62a}$$

$$J_2 = S_e(J_2)_e = S_e[M_e + \theta\Delta t(U_2 C + KD)_e]. \tag{62b}$$

The solution defined by equation (60) is then replaced by the sequence of two solutions,

$$J_2\{P\} = -\Delta t\{R\}^n, \quad J_1\{\Delta Q\} = \{P\}, \tag{63}$$

with $\{P\}$ the column matrix of the intermediate solution data. In the 'standard' matrix notation of Baker,[22] the coded form of equation (60a) is

$$\{R\} \equiv S_e\{R\}_e,$$

$$\{R\}_e \equiv \mathrm{DET}_e[\mathrm{B200}](\{Q\}^p_{n+1} - \{Q\}_n)_e + \Delta t\Big(-\{U\mathrm{BAR}K\}^{\mathrm{T}}[\mathrm{B30}K0]$$

$$+ \frac{K_e}{\mathrm{DET}_e}(\mathrm{ETA}KJ)_e(\mathrm{ETA}LJ)_e[\mathrm{B2}KL]\Big)(\theta\{Q\}^p_{n+1} + (1-\theta)\{Q\}_n)_e, \tag{64}$$

where repeated indices (K, J, L) are summed over n, the dimension of R^n. Further, $(\mathrm{EKA}KJ)_e$ and $(\mathrm{ETA}LJ)_e$ contain the element average values of the (four) components of the co-ordinate transformation $\partial\eta_k/\partial x_i$, recall equation (13), $\{U\mathrm{BAR}K\}_e$ contains the nodal values of the contravariant convection velocity (U, V, equation (16)), and DET_e is the element measure. Further, [B200] is the mass matrix, [B30K0], $1 \leqslant K \leqslant 2$, is the convection (hyper-) matrix and [B2KJ], $1 \leqslant (K, J) \leqslant 2$, is the diffusion matrix.

The Newton algorithm Jacobian for equation (64) is directly formed as,

$$J \equiv \frac{\partial\{R\}}{\partial\{Q\}} = S_e(J_e),$$

$$J_e = \mathrm{DET}_e[\mathrm{B200}] + \theta\Delta t\Big(-\{U\mathrm{BAR}K\}^{\mathrm{T}}_e[\mathrm{B30}K0]$$

$$+ \frac{K_e}{\mathrm{DET}_e}(\mathrm{ETA}KJ)_e(\mathrm{ETA}LJ)_e[\mathrm{B2}KL]\Big). \tag{65}$$

The tensor matrix product approximation to equation (65) is

$$J_{1e} = \mathrm{DET1}_e[\mathrm{A200}] - \theta\Delta t\{U\mathrm{BAR1}\}^{\mathrm{T}}[\mathrm{A3010}] + \frac{\theta\Delta t K_e}{\mathrm{DET1}_e}[\mathrm{A211}], \tag{66a}$$

$$J_{1e} = \mathrm{DET2}_e[\mathrm{A200}] - \theta\Delta t\{U\mathrm{BAR2}\}^{\mathrm{T}}[\mathrm{A3010}] + \frac{\theta\Delta t K_e}{\mathrm{DET2}_e}[\mathrm{A211}]. \tag{66b}$$

The tensor product of equations (66a, b) reproduces identically the first two terms in equation (65), the third term without the cross-derivatives and a truncation error term of mixed convection–diffusion products multiplied by Δt^2. Therefore, while equation (66) represent a decent approximation, the numerical linear algebra implementation will yield a linear convergence rate. Table II summarizes the measured convergence history for the sample problem, in terms of error in $\{\Delta Q\}$, which confirms convergence with four iterations to drive the error in $\{\Delta Q\}$ to 10^{-5}.

Table II. Convergence of tensor product Jacobian numerical linear algebra solution to equation (60)

	$(\Delta Q_c - \Delta Q_e)/\Delta Q_e^*$		
Iteration	Nodes 1, 4, 7	Nodes 2, 5, 8	Nodes 3, 6, 9
1	0·25875	0·00512	0
2	−0·05548	0·00038	0
3	0·01640	0·00000	0
4	0·00000	0·00000	0

* ΔQ_c = computed component of $\{\Delta Q\}$; ΔQ_e = exact component of $\{\Delta Q\}$, equation (60)

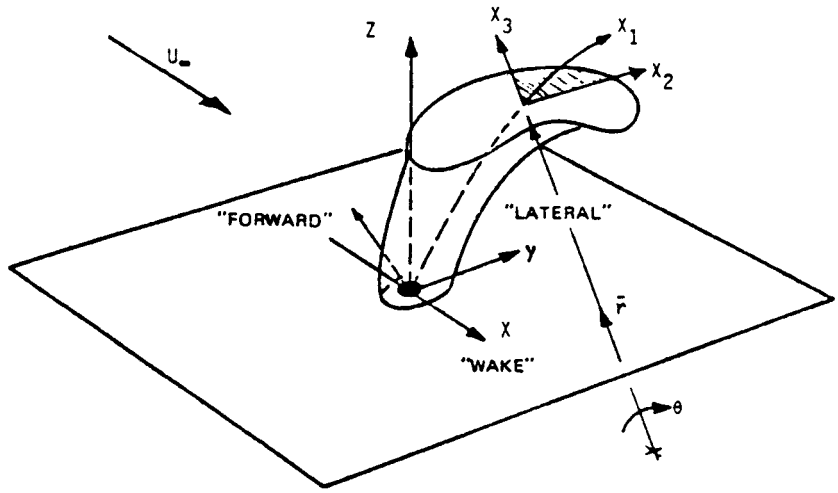

Figure 7. Schematic perspective of a jet in crossflow

A turbulent flow prediction

The TLNS equation system has found wide use in characterization of subsonic (including incompressible) flows in aerodynamics and/or hydrodynamics. In this instance, the axial pressure gradient is completely retarded (recall equation (18)) and problem definitions include juncture regions, internal duct flows and a variety of freejet configurations.[46] One recent application is the basic VSTOL jet definition, i.e. a relatively high-speed jet introduced prependicular into an imposed crossflow with boundary layer; see Figure 7. Results are reported[47] for $4 \leqslant R \leqslant 8$ circular jets. The steady 3D TLNS equation system is solved, equations (13)–(17), and the reported results employed the k–ε turbulent closure model system as defined in equations (10)–(12). The TLNS system is space-marched parallel to the jet axis, starting from an initial condition specification near the plate surface.

The essential physical characterizations of the VSTOL problem include:

(1) generation of a bluff jet cross-section (assuming an initially circular jet) with 'kidney-shaped' jet velocity isovels;
(2) self-generation of a transverse vortex pair within the jet cross-section that induces wake entrainment and migrates downstream and off-axis with increasing distance from the injection plane;

(3) generation of an intense ring of high levels of turbulent kinetic energy about the jet and elevated levels in the wake.

All essential characterization aspects are present in the TLNS solutions reported in Reference 47. For example, Figure 8(*a*) shows the composite three-dimensional velocity field on the transverse plane at $2\frac{1}{2}$ jet diameters above the injection plane. The vectors are parallel to the local transverse

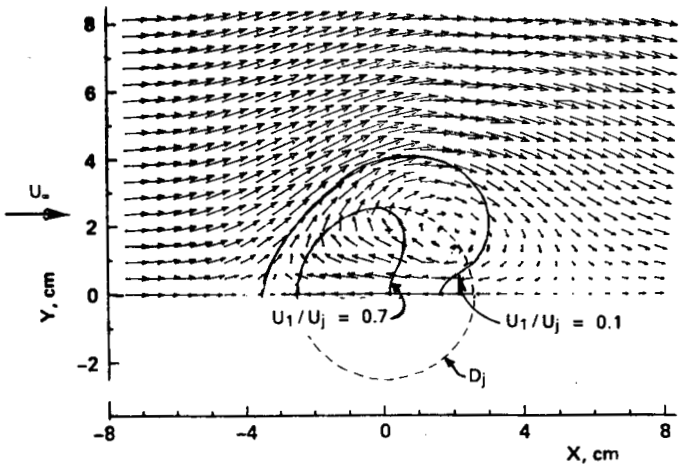

(a)

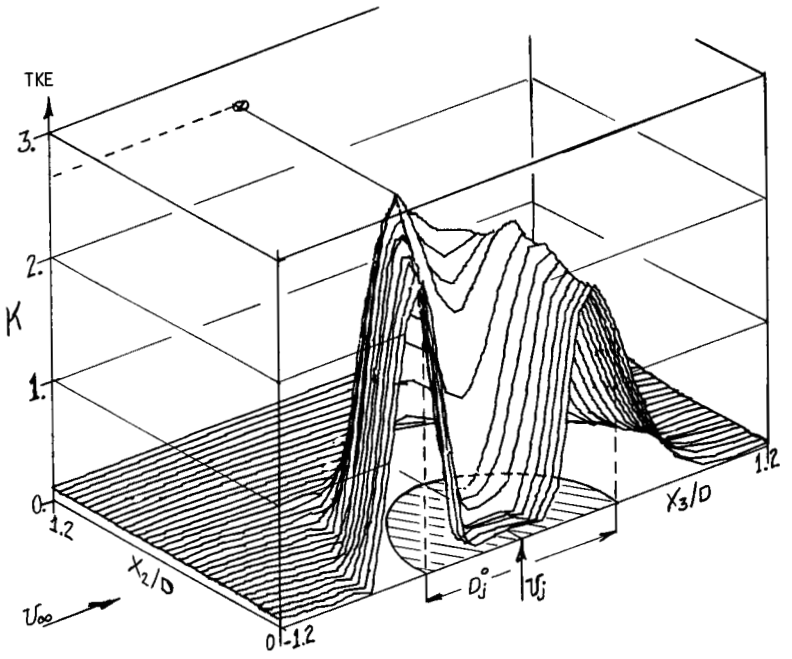

(b)

Figure 8. PNS algorithm prediction of three-dimensional turbulent jet in crossflow, velocity ratio = 8, $Z/D = 2{\cdot}4$ (from Baker and Orzechowski[47]). (a) Three dimensional mean velocity field; (b) Turbulent kinetic energy distribution

velocity, with tail located at each node of the transverse plane discretization. The contours are the intersection of the jet velocity isovel surfaces with the plane, with level normalized by the initial jet velocity. The broken circle denotes the relative location of the injection orifice. The self-induced vortex is centred in the lobe of the kidney-shaped isovel, and the mechanisms of lateral deflection, forward stagnation and wake entrainment are clearly illustrated. Figure 8(*b*) is a surface plot of the computed distribution of turbulent kinetic energy at the same location, which illustrates creation of a high-intensity ring and elevated wake levels from the (assumed) uniform background. Detailed comparisons with experimental data are contained in the cited reference.

CONCLUSIONS

A Taylor weak statement (TWS) theory has been constructed for viscous compressible and turbulent aerodynamic flow applications, for coincident construction of stability mechanisms within the classic Galerkin finite element weak statement of semi-discrete approximation error orthogonalization. Recovery of over a dozen independently derived CFD algorithms occurs within the TWS theory, with the important addition of a general implicit construction for rapid convergence to steady state. Confirmation of the theoretical asymptotic error estimates was achieved for a supersonic inviscid shocked flow and a viscous boundary layer flow. The latter also indicated a significant improvement in accuracy level attainable with use of a quadratic finite element trial space. Verification of a factored tensor matrix product numerical linear algebra approximation to a Newton algorithm was achieved as well as implementation of a k–ε closure model in the TLNS equation system algorithm.

ACKNOWLEDGEMENTS

The work reported herein was principally supported by NASA Langley Research Center under Grant NAGI-319. Additional support has been provided by NASA Ames Research Center under SBIR Contract NAS2-12347 and the U. S. Naval Air Development Center, Contract N62669-84C-0264. Further financial support was provided by the Computational Fluid Dynamics Laboratory, the generosity of the corporate sustaining members of which is gratefully acknowledged.

REFERENCES

1. S. G. Rubin, 'Incompressible flow along a corner', *J. Fluid Mech.*, **26,** 97–110 (1966).
2. S. G. Rubin and B. Grossman, 'Viscous flow along the corner: numerical solution of the corner layer equations', *J. Q. Appl. Math.*, **29,** 169–186 (1971).
3. A. Pal and S. G. Rubin, 'Asymptotic features of viscous flow along a corner', *J. A. Appl. Math.*, **27,** 99–108 (1971).
4. B. C. Weinberg and S. G. Rubin, 'Compressible corner flow', *J. Fluid Mech.*, **56,** 753–774 (1972).
5. T. C. Lin and S. G. Rubin, 'Viscous flow over a cone at moderate incidence', *J. Comput. Fluids*, **1,** 37–57 (1973).
6. S. G. Rubin, 'A review of marching procedures for parabolized Navier–Stokes equations', *Numerical and Physical Aspects of Aerodynamic Flows*, Springer-Verlag, Berlin, pp. 171–186, 1982.
7. A. Lin and S. G. Rubin, 'Three-dimensional supersonic viscous flow over a cone at incidence, *AIAA J.*, **20,** 1500–1507 (1982).
8. D. R. Reddy and S. G. Rubin, 'Subsonic/transonic, viscous/inviscid relaxation procedures for strong pressure interactions', *Technical Paper AIAA-84-1627*, 1984.
9. Y. C. Vigneron, J. V. Rakich and J. C. Tannehill, 'Calculation of supersonic viscous flow over delta wings with sharp subsonic leading edges', *Technical Paper AIAA-78-1137*, 1978.
10. J. V. Rakich, Y. C. Vigneron and R. Agarwal, 'Computation of supersonic viscous flows over ogive-cylinders at angle of attack', *Technical Paper AIAA-79-0131*, 1979.
11. J. C. Tannehill, E. Venkatapathy and J. V. Rakich, 'Numerical solution of supersonic viscous flow over blunt delta wings', *AIAA J.*, **20,** 203–210 (1981).
12. L. B. Schiff and J. L. Steger, 'Numerical simulation of steady supersonic viscous flow', *AIAA J.*, **18,** 1421–1430 (1980).
13. D. S. Chaussee, J. L. Patterson, P. Kutler, T. H. Pulliam and J. L. Steger, 'A numerical simulation of hypersonic viscous flows over arbitrary geometries at high angle of attack', *Technical Paper AIAA-81-0050*, 1981.

14. S. P. Shanks, G. R. Srinivasan and W. E. Nicolet, 'AFWAL parabolized Navier–Stokes code: formulation and user's manual', *Technical Report AFWAL-TR-82-3034*, 1982.
15. J. V. Rakich, 'Iterative PNS method for attached flows with upstream influence', *Technical Paper AIAA-83-1955*, 1983.
16. W. R. Briley and H. McDonald, 'Solution of the multidimensional compressible Navier–Stokes equations by a generalized implicit method', *J. Comput. Phys.*, **24**, 372–397 (1977).
17. W. R. Briley and H. McDonald, 'Analysis and computation of viscous subsonic primary and secondary flows', *Technical Paper AIAA-79-1453*, 1979.
18. J. P. Kreskovsky, W. R. Briley and H. McDonald, 'Investigation of mixing in a turbofan exhaust duct, part I: analysis and computation procedure', *AIAA J.*, **22**, 374–382 (1984).
19. L. A. Povinelli, B. H. Anderson, and W. H. Gerstenmaier, 'Computation of three-dimensional flow in turbofan mixers and comparison with experimental data', *Technical Report NASA TM-81410*, 1980.
20. B. E. Launder and D. B. Spalding, 'The numerical computation of turbulent flows', *Comput. Methods Appl. Mech. Eng.*, **3**, 269–289 (1974).
21. A. J. Baker and J. A. Orzechowski, 'An interaction algorithm for three-dimensional turbulent subsonic aerodynamic juncture region flow', *AIAA J.*, **21**, 524–533 (1983).
22. A. J. Baker, *Finite Element Computational Fluid Mechanics*, McGraw-Hill/Hemisphere, New York, 1983.
23. A. J. Baker, 'Review: a finite element penalty algorithm for the parabolic Navier–Stokes equations for turbulent three-dimensional flow', *Comput. Methods Appl. Mech. Eng.*, **46**, 277–293 (1984).
24. T. Cebeci and A. M. O. Smith, *Analysis of Turbulent Boundary Layers*, Academic Press, New York, 1974.
25. J. C. Tannehill and R. A. Mohling, 'Development of equilibrium air computer programs suitable for numerical computation using time-dependent or shock-capturing methods', *Technical Report NASA-CR-2134*, 1972.
26. B. J. Daly and F. H. Harlow, 'Transport equations of turbulence', *Phys. Fluids*, **31**, 2634, 1970.
27. B. E. Launder, G. J. Reece and W. Rodi, 'Progress in the development of Reynolds stress turbulence closure', *J. Fluid Mech.*, **68**, 537–566 (1975).
28. W. Rodi, *Turbulence Models and Their Application in Hydraulics—A State of the Art Review*, IAHR Publication, Delft, Holland, 1980.
29. A. J. Baker and J. W. Kim, 'A Taylor weak-statement algorithm for hyperbolic conservation laws', *Int. j. numer. methods fluids*, **7**, 489–520 (1987).
30. R. W. Walters, 'LU methods for the compressible Navier–Stokes equations', *Ph.D. Thesis*, N. Carolina State University, Raleigh, NC, 1984.
31. R. W. Walters and D. L. Dwoyer, 'Efficient solutions to the Euler equations for supersonic flow with embedded subsonic regions', *Technical Paper NASA* 2523, 1987.
32. J. L. Thomas, B. van Leer and R. W. Walters, 'Implicit flux-split schemes for the Euler equations', *Technical Paper AIAA 85-1680*, 1985.
33. J. T. Oden and J. N. Reddy, *An Introduction to the Mathematical Theory of Finite Elements*, Wiley, New York, 1976.
34. P. D. Lax and B. Wendroff, 'Systems of conservation laws', *Commun. Pure Appl. Math.*, **13**, 217–237 (1960).
35. J. Donea, 'A Taylor–Galerkin method for convective transport problems', *Int. j. numer. methods eng.*, **20**, 101–119 (1984).
36. J. Donea, S. Giuliani, H. Laval and L. Quartapelle, 'Time-accurate solution of advection–diffusion problems by finite elements', *J. Comput. Methods Appl. Mech. Eng.*, **45**, 123–145 (1984).
37. K. W. Morton and A. K. Parrott, 'Generalized Galerkin methods for first order hyperbolic equations', *J. Comput. Phys.*, **36**, 249–270 (1980).
38. K. W. Morton, 'Characteristic Galerkin methods for hyperbolic problems', *Proc. 5th GAMM Conf. on Numerical Methods in Fluid Mechanics*, Rome, 1983.
39. R. Lohner, K. Morgan and O. C. Zienkiewicz, 'The solution of non-linear hyperbolic equation systems by the finite element method', *Int. j. numer. methods fluids*, **4**, 1043–1063 (1984).
40. R. Lohner, K. Morgan and O. C. Zienkiewicz, 'An adaptive finite element procedure for compressible high speed flows', *Comput. Methods Appl. Mech. Eng.*, **51**, 441–465 (1985).
41. L. B. Wahlbin, 'A dissipative Galerkin method applied to some quasi-linear Hyperbolic equations', *R.A.I.R.O.*, **8**, 109–117 (1974).
42. J. E. Dendy, 'Two methods of Galerkin type achieving optimum L^2 rates of convergence for first-order hyperbolics', *SIAM J. Numer. Anal.*, **11**, 637–653 (1974).
43. W. H. Raymond and A. Garder, 'Selective damping in a Galerkin method for solving wave problems with variables grids', *Mon. Weather Rev.*, **104**, 1583–1590 (1976).
44. T. J. R. Hughes and A. N. Brooks, 'A multidimensional upwind scheme with no crosswind diffusion', in T. J. R. Hughes (ed.) *Finite Element Methods for Convection Dominated Flows*, ASME, AMD-34, New York, 1979, pp. 19–35.
45. A. J. Baker and M. O. Soliman, 'A finite element algorithm for computational fluid dynamics', *AIAA J.*, **21**, 816–827 (1983).
46. A. J. Baker, 'On a penalty finite element CFD algorithm for high speed flow', *Comput. Methods Appl. Mech. Eng.*, **51**, 395–420 (1985).
47. A. J. Baker and J. A. Orzechowski, 'Prediction of turbulent near-field evolution of a jet in crossflow using a PNS solver', *U.S. Navy Technical Report NADC-86076-60*, 1986.